NANO LETTERS

pubs.acs.org/NanoLett Letter

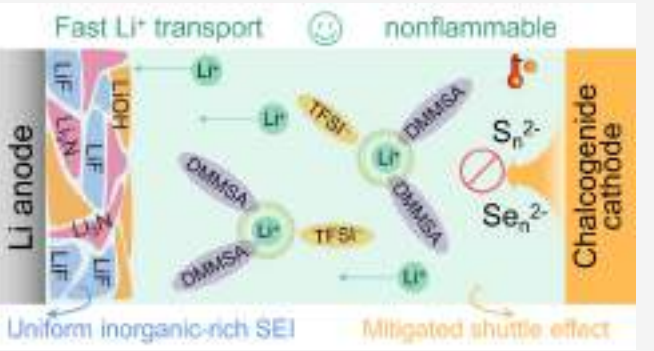
Reversible High-Temperature Lithium–Chalcogenide Batteries Enabled by a Nonflammable Sulfonamide Deep Eutectic Electrolyte

Panpan Dong, Xuemeng Gan, Liangjie Gu, Ting Yang, Muqiao Su, Min-Kyu Song,* and Weiqing Yang*

Cite This: *Nano Lett.* 2026, 26, 11538–11547 Read Online

ACCESS | Metrics & More | Article Recommendations | Supporting Information

ABSTRACT: Significant efforts have recently been dedicated to enhancing reversibility and safety of high-temperature lithium–chalcogenide batteries (LCBs) to address performance-limiting issues. However, bottlenecks in electrolyte design that severely constrain the utilization of active material and reversibility of a lithium anode at elevated temperatures have received little attention. Herein, we report a nonflammable sulfonamide deep eutectic electrolyte (SDEE) composed of *N*,*N*-dimethylmethanesulfonamide and lithium bis(trifluoromethanesulfonyl)imide for high-temperature LCBs. The SDEE exhibits good thermal stability, high lithium-ion transference number, and a wide electrochemical window. Additionally, SDEE facilitates the formation of a compact and uniform lithium deposition, leading to a much mitigated shuttle effect and improved reversibility of the lithium anode compared to an ether-based electrolyte. LCBs with an SDEE exhibit a low overcharging degree at 60 °C (8.4%) and a high specific capacity (~1107 mAh g^{-1}) at 328.2 mA g^{-1}. This work offers a viable electrolyte design concept for safe batteries targeting elevated temperatures using high-capacity electrodes.



KEYWORDS: *lithium–chalcogenide batteries, sulfonamide deep eutectic electrolyte, shuttle effect, elevated temperatures*

The rapid advancement of energy storage technologies has intensified the demand for safe, high-energy-density batteries capable of stable operation under diverse conditions.[1−3] Lithium–chalcogenide batteries (LCBs), including lithium–sulfur (Li–S), lithium–selenium (Li–Se), and lithium–selenium sulfide (Li–Se_mS_n) batteries, have emerged as promising candidates due to their ultrahigh theoretical energy density, low weight, abundant resources, and environmental friendliness.[4,5] Nevertheless, LCBs suffer from rapid capacity decay and poor reversibility of the lithium metal anode, primarily caused by active material dissolution and shuttling of redox intermediates during cycling.[6,7] Significant research efforts have been conducted to improve LCBs' performance through strategies such as electrode design,[8,9] separator modification,[10,11] electrolyte engineering,[12,13] and lithium anode stabilization.[14,15] Recently, Jung et al. demonstrated that a low-polarity ether electrolyte effectively suppresses parasitic reactions between lithium metal and polysulfides, promoting uniform Li deposition and stabilizing the lithium anode in Li–S batteries.[16] Kim et al. revealed that Se in SeS_2 cathodes acts as a nucleation site catalyzing S growth for enhanced battery performance.[17] These mechanistic insights highlight the importance of electrolyte engineering for LCBs with sulfur/selenium-based cathodes. While these advances have primarily focused on operation at ambient temperatures, research on LCBs operating at elevated temperatures (>50 °C) remains scarce. This limitation hinders their practical application in demanding industrial settings, such as oil exploration.

Achieving high-performance LCBs with good safety at elevated temperatures is hindered by two main factors. First, although elevated temperatures accelerate redox kinetics and reduce overpotential, they inevitably intensify the dissolution of active materials and the polysulfide/polyselenide shuttle effect in ether-based electrolytes, directly causing rapid capacity fade and irreversible degradation of the lithium metal anode.[18] Second, the high volatility and flammability of ether solvents, due to their intrinsically low boiling and flash points, pose severe safety hazards under >50 °C operation, which is a risk that cannot be overcome by electrode or separator design alone. While advanced cathode hosts[19] and multifunctional separators[20] have improved cycling behavior to some extent, these approaches still rely on ether electrolytes[21,22] and therefore fail to eliminate either the shuttle effect or the flammability at the electrolyte level. Consequently, an electrolyte that is inherently nonflammable and simultaneously

Received: June 24, 2026
Revised: August 14, 2026
Accepted: August 17, 2026
Published: August 20, 2026



ACS Publications © 2026 American Chemical Society

https://doi.org/10.1021/acs.nanolett.6c03111
Nano Lett. 2026, 26, 11538–11547

Downloaded from pubs.acs.org/naleft/article-pdf/26/34/11538/6946057/acs.nanolett.6c03111.pdf by SOUTHWEST JIAOTONG UNIV user on 07 November 2026

capable of suppressing the shuttle while significantly improving the reversibility of Li plating/stripping remains an urgent but unmet need.

Recent studies on alternative electrolytes for high-temperature LCBs focus on three dominant strategies: solid-state electrolytes (SEEs),[23,24] ionic liquids (ILs),[25,26] and deep eutectic electrolytes (DEEs).[27,28] SSEs offer excellent thermal stability but suffer from rigid solid−solid contact that leads to increasing interfacial impedance during cycling.[29] ILs provide good interfacial wettability with electrodes and a wide electrochemical stability window, yet their practical use is limited by high cost and poor compatibility with lithium metal anodes.[30,31] In contrast, DEEs exhibit nonflammability and low cost, making them attractive for wide-temperature lithium batteries.[32,33] However, most studies on DEEs have predominantly reported on transition-metal oxide cathodes. The potential of DEEs to concurrently resolve the safety and shuttle challenges specific to LCBs has not been investigated. This unexplored direction represents a critical gap because the dissolved polysulfides/polyselenides in LCBs impose far more stringent requirements on electrolyte solvation structure than conventional intercalation cathodes.

Herein, we report a nonflammable sulfonamide deep eutectic electrolyte (SDEE) specifically designed to fill this gap and simultaneously address the safety and shuttle-induced irreversibility of high-temperature LCBs. The SDEE is composed of *N*,*N*-dimethylmethanesulfonamide (DMMSA) and lithium bis(trifluoromethanesulfonyl)imide (LiTFSI). DMMSA was selected as a nonfluorinated, cost-effective sulfonamide that provides a deliberately moderate Li^+ solvation, which is essential to simultaneously ensure complete salt dissociation and suppress the polysulfide/polyselenide shuttle in high-temperature LCBs. Through a combination of theoretical calculations and systematic experimental characterizations, we investigate the lithium-ion solvation structure of an SDEE and its influence on the lithium deposition morphology, active material dissolution, and polysulfide/polyselenide shuttle behavior. The overarching objective is to elucidate how a moderate solvation environment can suppress the shuttle effect while enabling significantly improved reversibility of lithium plating/stripping, thereby establishing a rational electrolyte design principle for safe LCB operation at elevated temperatures.

Figure 1 illustrates the challenges for LCBs operated at elevated temperatures. In this work, an ether-based electrolyte composed of 1 M lithium bis(trifluoromethanesulfonyl) imide (LiTFSI) in 1,3-dioxolane (DOL) and 1,2-dimethoxyethane (DME) was studied as the reference electrolyte. At high temperatures, LCBs with a conventional ether-based electrolyte exhibit severe dissolution of active materials, leading to poor utilization of the active material and rapid capacity loss (Figure 1a). The shuttle effect of redox intermediates in an ether-based electrolyte further results in degradation of the lithium metal anode due to severe side reactions between polysulfides/polyselenides and lithium metal. These behaviors greatly affect the durability and reversibility of high-temperature LCBs. In contrast, as shown in Figure 1b, the nonflammable SDEE exhibits a wide temperature range of −40 to 100 °C and wide electrochemical stability window (Figure S1, Supporting Information), suggesting great potential in high-temperature LCBs. Additionally, a selenium sulfide (Se_mS_n) electrode in an SDEE shows less color change after being immersed in an SDEE at 60 °C for 24 h when

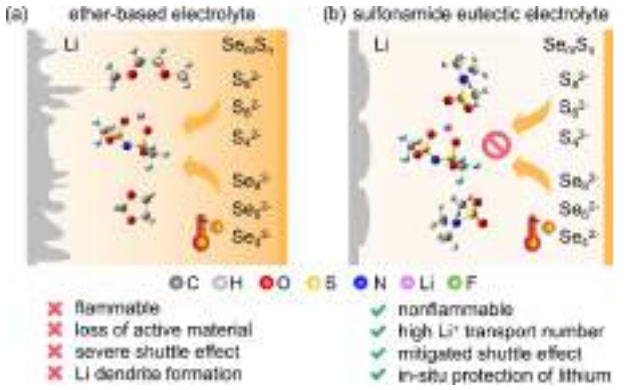


Figure 1. Challenges for durable high-temperature lithium−chalcogenide batteries (LCBs). (a) With conventional ether-based electrolytes, severe dissolution of active materials and an intermediate shuttle effect in electrolytes at high temperature lead to rapid loss of capacity. Challenges in the Li metal anode come from the severe side reactions between polysulfides/polyselenides and active lithium, forming mossy/dead Li and poor Coulombic efficiency. (b) The nonflammable sulfonamide eutectic electrolyte (SDEE) can mitigate dissolution/diffusion of the active material and redox intermediates. The SDEE also facilitates the formation of compact uniform Li at high temperature, thus enabling an improved reversibility of the Li metal anode.

compared to the one in an ether-based electrolyte (Figure S2, Supporting Information), indicating less dissolution of active material in the SDEE. Moreover, the SDEE exhibits a high lithium-ion transference number, which suggests the formation of compact, uniform lithium deposition and thus improves the reversibility of lithium anodes in high-temperature LCBs.

The miscibility and ionic transport properties of the SDEE were systematically tuned by varying the molar ratio of DMMSA to LiTFSI (Figure S3, Supporting Information). At a ratio of 2:1, macroscopic phase separation was evident, indicating insufficient coordination of Li^+ by DMMSA to form a homogeneous phase. Upon increasing the ratio to 4:1 and 6:1, transparent and homogeneous electrolytes were readily obtained. The measured densities of these homogeneous electrolytes were in the range of 1.3−1.4 g mL^{-1} (Figure S4, Supporting Information), which is slightly above the 1.3 g mL^{-1} benchmark typically desired for high-energy-density, lean-electrolyte cells.[34,35] However, the ionic conductivity exhibited a monotonic decline with increasing DMMSA content, attributed to the dilution of LiTFSI. Consequently, the DMMSA:LiTFSI molar ratio of 4:1 was established as the optimal composition, representing the minimal DMMSA content required to ensure complete miscibility while maximizing ionic conductivity. Besides, the SDEE electrolyte shows a much lower density than that of a lithium-doped ionic liquid electrolyte (Li@IL, 1.55 g mL^{-1}). To address the density criterion in future iterations, the incorporation of a fluorinated ether diluent, specifically 1,1,2,2-tetrafluoroethyl-2,2,3,3-tetrafluoropropyl ether, is proposed to reduce the overall density further while tuning the solvation structure for enhanced electrochemical stability. Moreover, other sulfonamides with different functional groups (e.g., varying alkyl chain lengths, fluorinated substituents, and asymmetric structures) will be explored to elucidate structure−property relationships for high-temperature LCBs.

A comprehensive understanding of the ion solvation structure is critical for rational electrolyte design in high-

https://doi.org/10.1021/acs.nanolett.6c03111
Nano Lett. 2026, 26, 11538−11547

Downloaded from pubs.acs.org/naletd/article-pdf/26/34/11538/6946057/acs.nanolett.6c03111.pdf by SOUTHWEST JIAOTONG UNIV user on 07 November 2026

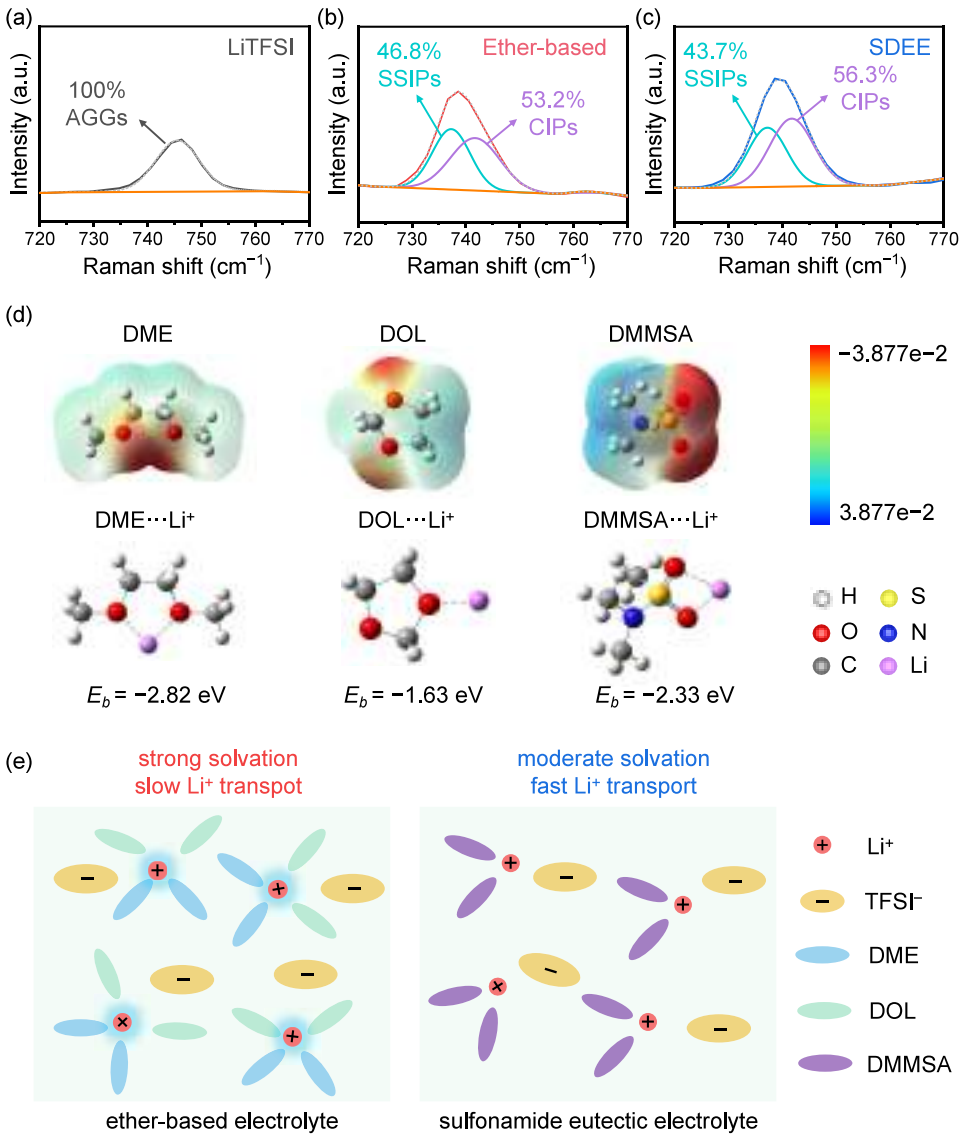


Figure 2. Lithium-ion solvation structures of the SDEE. Raman spectra of (a) solid LiTFSI, (b) ether-based electrolyte (LiTFSI-DOL/DME), and (c) SDEE (LiTFSI-DMMSA). Note: AGGs, SSIPs, and CIPs refer to ion aggregates, solvent-separated ion pairs, and contact ion pairs, respectively. (d) Electrostatic potential (ESP) of DME, DOL, and DMMSA and the binding energy (E_b) of DME-Li^+, DOL-Li^+, and DMMSA-Li^+. (e) Proposed Li^+ ion solvation structures in ether-based and SDEE electrolytes.

performance LCBs. Raman spectroscopy was performed to quantify the proportions of ion-pair aggregates (AGGs), solvent-separated ion pairs (SSIPs), and contact ion pairs (CIPs) in ether-based and SDEE electrolytes (Figure 2a–c). The S–N–S symmetric stretching vibration band of $TFSI^-$ shows complete disappearance of the AGGs[36] (~746 cm^{-1}) in both ether-based (LiTFSI-DOL/DME) and SDEE (LiTFSI-DMMSA) electrolytes, indicating full Li^+ solvation. Deconvolution of the remaining bands into SSIPs (~737 cm^{-1}) and CIPs (~741 cm^{-1}) reveals a higher CIP fraction in the SDEE (56.3%) than in the ether electrolyte (53.2%), indicating that DMMSA promotes CIP formation. To verify whether this CIP-dominated solvation persists at practical operating temperatures, temperature-dependent Raman spectra were collected from 30 to 80 °C (Figures S5–S7, Supporting Information). In the ether electrolyte, the peak shifts to higher wavenumbers and the AGG fraction surges to 45.9% at 60 °C, attributable to solvent evaporation and consequent desolvation. In sharp contrast, the SDEE exhibits no discernible peak shift and retains a high CIP proportion (67.5%) with only a moderate AGG fraction (24.6%) at 60 °C. These results suggest that the SDEE maintains a stable, CIP-dominated solvation structure at elevated temperatures, which is favorable for uniform Li deposition and electrolyte stability as previously reported.[37]

To further investigate the Li^+ ion solvation structure in ether-based and SDEE electrolytes, we performed density functional theory (DFT) calculations. According to the surface electrostatic potential (ESP) distribution and binding energy (E_b) of different solvents toward the Li^+ ion (Figure 2d), the binding energy of different solvents toward the Li^+ ion follows the decreasing order (eV) DME-Li^+ (−2.82) > DMMSA-Li^+ (−2.33) > DOL-Li^+ (−1.63). In ether-based electrolyte, the double O atoms of DME exhibit strong binding to lithium ions with an average bond length of 1.86 Å (Figure S8, Supporting Information), demonstrating the strong solvating ability of DME to Li^+ (i.e., SSIPs dominant) as previously reported.[38] In contrast, DMMSA-Li^+ exhibits a middle binding energy but

https://doi.org/10.1021/acs.nanolett.6c03111
Nano Lett. 2026, 26, 11538−11547

Downloaded from pubs.acs.org/naleft/article-pdf/26/34/11538/6946057/acs.nanolett.6c03111.pdf by SOUTHWEST JIAOTONG UNIV user on 07 November 2026

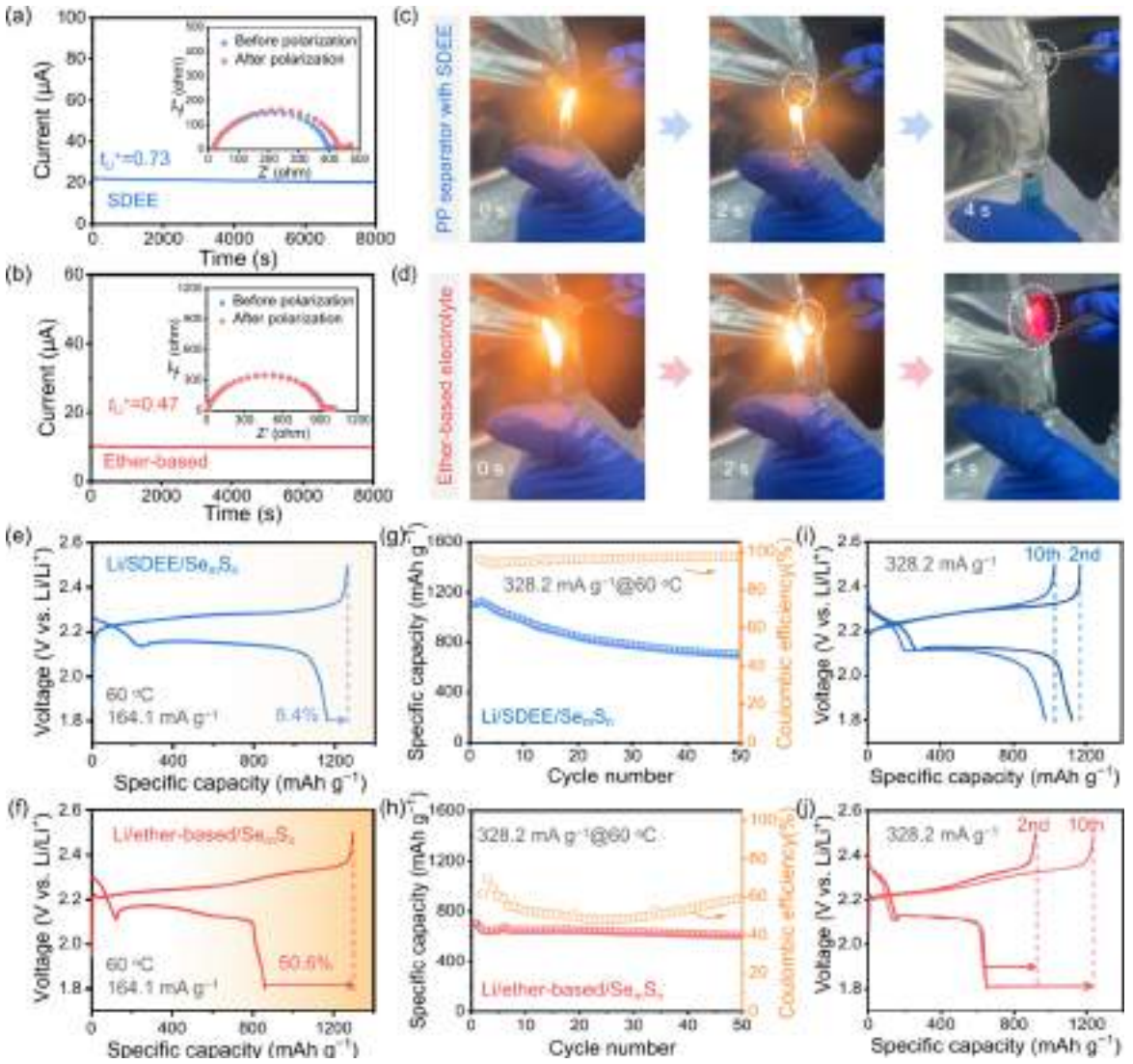


Figure 3. Characterizations of the SDEE and electrochemical performances of LCBs with an SDEE. Lithium-ion transference number of (a) SDEE and (b) ether-based electrolytes. Flammability tests of polypropylene (PP) separators soaked with (c) SDEE and (d) ether-based electrolytes. Comparison of electrochemical performance of LCBs with SDEE and ether-based electrolytes at 60 °C. (e, f) Initial voltage profiles at 164.1 mA g^{-1}. (g, h) Cycling performance and (i, j) voltage profiles of the second and tenth cycles at 328.2 mA g^{-1}.

much longer average bond length of 2.00 Å when compared to DME-Li$^+$ and DOL-Li$^+$, indicating a more facile desolvation ability of Li$^+$ by DMMSA (i.e., CIPs dominant). These results correspond well with Raman spectral analysis. As a result, the ether-based electrolyte is dominated by SSIPs (Figure 2e), while the SDEE is prominently CIPs, indicating the DMMSA molecule provides moderate Li$^+$ ion solvation and enhances CIP formation. Such a moderate Li$^+$ solvation structure in the SDEE can effectively facilitate Li$^+$ ion transport, which is conducive to the formation of uniform lithium deposition during cycling. Additionally, the electrochemical stability of solvents and solvation clusters in SDEE and ether-based electrolytes was further analyzed by DFT-calculated molecular orbital energy levels (Figure S9, Supporting Information). DMMSA shows a lower HOMO (i.e., the highest occupied molecular orbital) energy level than that of DME and DOL, indicating better oxidation stability. However, the DOL-Li$^+$ cluster shows the lowest LUMO (i.e., the lowest unoccupied molecular orbital) and the highest HOMO compared to DME-Li$^+$ and DMMSA-Li$^+$, which is susceptible to reduction and decomposition. This result often leads to the formation of an unstable organic-rich solid-electrolyte interphase (SEI) layer, thus resulting in degradation of the lithium metal anode and impairing battery performance in an ether-based electrolyte.

The ion solvation structure of an electrolyte greatly affects its electrochemical property especially at elevated temperatures. To evaluate the diffusion and mobility of Li$^+$ ions, lithium-ion transference number (t_{Li}^+) measurement of an SDEE electrolyte was performed at 60 °C. As shown in Figure 3a,b, the SDEE exhibits a higher t_{Li}^+ of 0.73 than that of ether-based electrolyte (0.47), which is well consistent with the above Raman analysis and DFT calculations. This result suggests fast lithium ion transport in the SDEE due to the facile desolvation ability of Li$^+$ by DMMSA, which is beneficial in the formation of uniform lithium deposition and an anion-derived SEI layer on lithium metal. The Li@IL electrolyte is nonflammable, confirming its suitability as a benchmark devoid of evaporation artifacts. However, the Li@IL shows a much lower t_{Li}^+ of 0.13 than that of SDEE (0.73) because of the large size of ionic liquid cations (Figure S10, Supporting

https://doi.org/10.1021/acs.nanolett.6c03111
Nano Lett. 2026, 26, 11538−11547

Downloaded from pubs.acs.org/naleft/article-pdf/26/34/11538/6946057/acs.nanolett.6c03111.pdf by SOUTHWEST JIAOTONG UNIV user on 07 November 2026

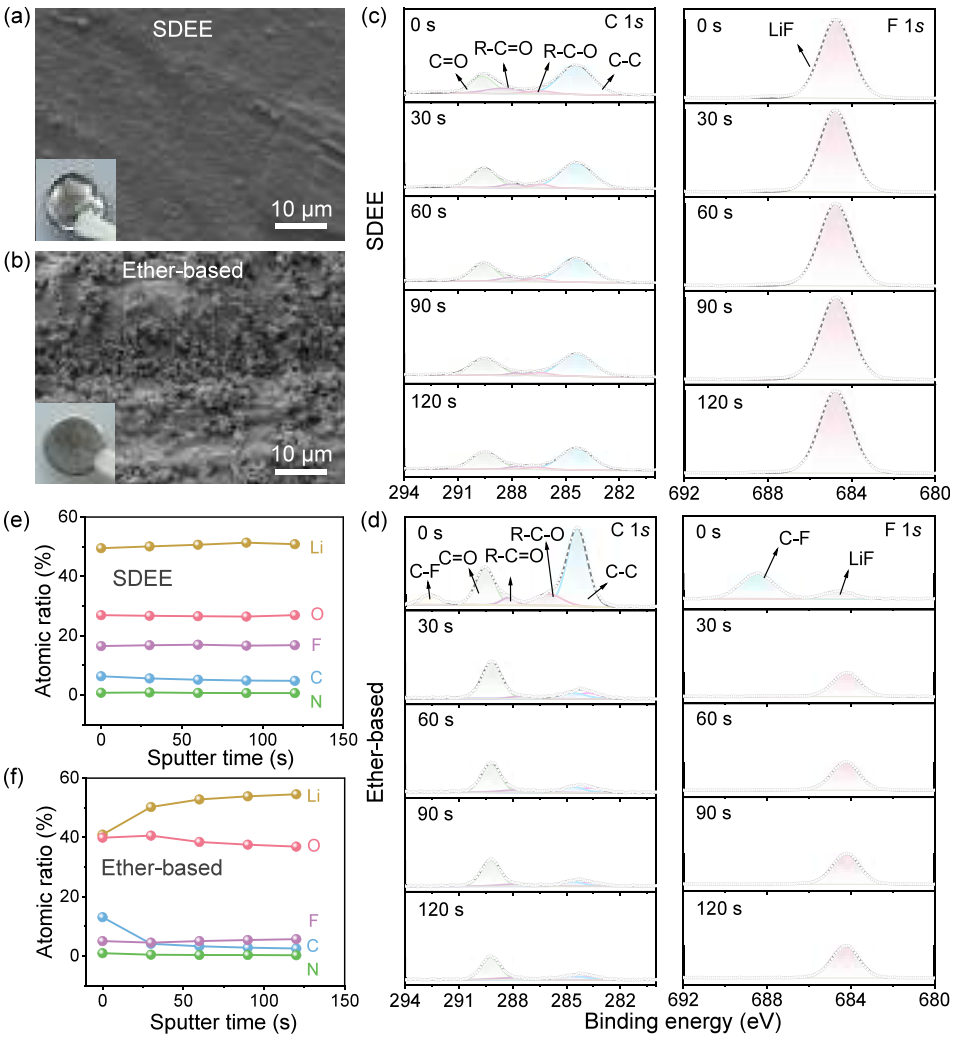


Figure 4. Morphology and surface chemistry of Li metal anodes with different electrolytes. SEM images of Li anodes in Li/Li cells with (a) SDEE and (b) ether-based electrolytes. The insets are optical photos of Li anodes. The Li/Li cells were tested at 0.25 mA cm^{-2} and 0.25 mAh cm^{-2} at 60 °C for 10 cycles. XPS depth profiles of C 1s and F 1s spectra of cycled Li metal anodes with (c) SDEE and (d) ether-based electrolytes. The evolution of elemental contents after different sputtering times of Li metal anodes with (e) SDEE and (f) ether-based electrolytes.

Information). Additionally, we conducted a comparative flammability test to evaluate the thermal stability of the SDEE, a conventional ether-based electrolyte, and a Li@IL electrolyte. The polypropylene (PP) separator soaked with SDEE and Li@IL cannot be ignited (Figure 3c and Figure S11, Supporting Information), suggesting good thermal stability and nonflammability of the SDEE and Li@IL. In contrast, the PP separator soaked with an ether-based electrolyte burns with a visible flame right after ignition (Figure 3d) due to the flammable nature of DME and DOL solvents, indicating potential safety risks of ether-based electrolytes when used at high temperatures.

To further demonstrate the electrochemical performance of the SDEE in high-temperature LCBs, a selenium sulfide (Se_mS_n) cathode was synthesized (Figure S12, Supporting Information) and tested at 60 °C. The stoichiometric composition of Se_mS_n was calculated as 0.67:17.68 (Table S1, Supporting Information). In the work, Se_mS_n refers to $Se_{0.67}S_{17.68}$ unless otherwise stated. When tested at a low current density of 164.1 mA g^{-1}, the Li/Se_mS_n cell with the SDEE exhibits a higher specific capacity (~1165 mAh g^{-1}, Figure 3e) than that of a Li/Se_mS_n cell with an ether-based electrolyte (~861 mAh g^{-1}, Figure 3f) and Li@IL electrolyte (~923 mAh g^{-1}, Figure S13 in the Supporting Information), suggesting much improved utilization of active material in the SDEE. Additionally, the SDEE-based cell shows a smaller overcharging degree (8.4%), while the ether-based electrolyte cell shows a high overcharging degree of 50.6%, which is attributed to severe dissolution and diffusion of redox intermediates in a conventional ether-based electrolyte at 60 °C. Furthermore, the Li/Se_mS_n cell with the SDEE delivers a specific capacity of ~1107 mAh g^{-1} at 328.2 mA g^{-1} with a high Coulombic efficiency (CE) of 97.2% after 50 cycles (Figure 3g,i). The Li/Se_mS_n cell with Li@IL achieves a specific capacity of ~861 mAh g^{-1} at 328.2 mA g^{-1} with an average CE of ~97% after 50 cycles (Figure S14, Supporting Information). These results demonstrate that under thermally stable and nonvolatile conditions, the SDEE substantially outperforms a representative ionic liquid electrolyte in terms of active material utilization. In contrast, the Li/Se_mS_n cell with an ether-based electrolyte exhibits a discharge capacity (~700 mAh g^{-1}) with a low CE < 60% (Figure 3h, 3j), indicating a continuous shuttle effect of polysulfides/polyselenides during cycling. The comparison of the SDEE and previously reported

https://doi.org/10.1021/acs.nanolett.6c03111
Nano Lett. 2026, 26, 11538−11547

Downloaded from pubs.acs.org/naleftd/article-pdf/26/34/11538/6946057/acs.nanolett.6c03111.pdf by SOUTHWEST JIAOTONG UNIV user on 07 November 2026

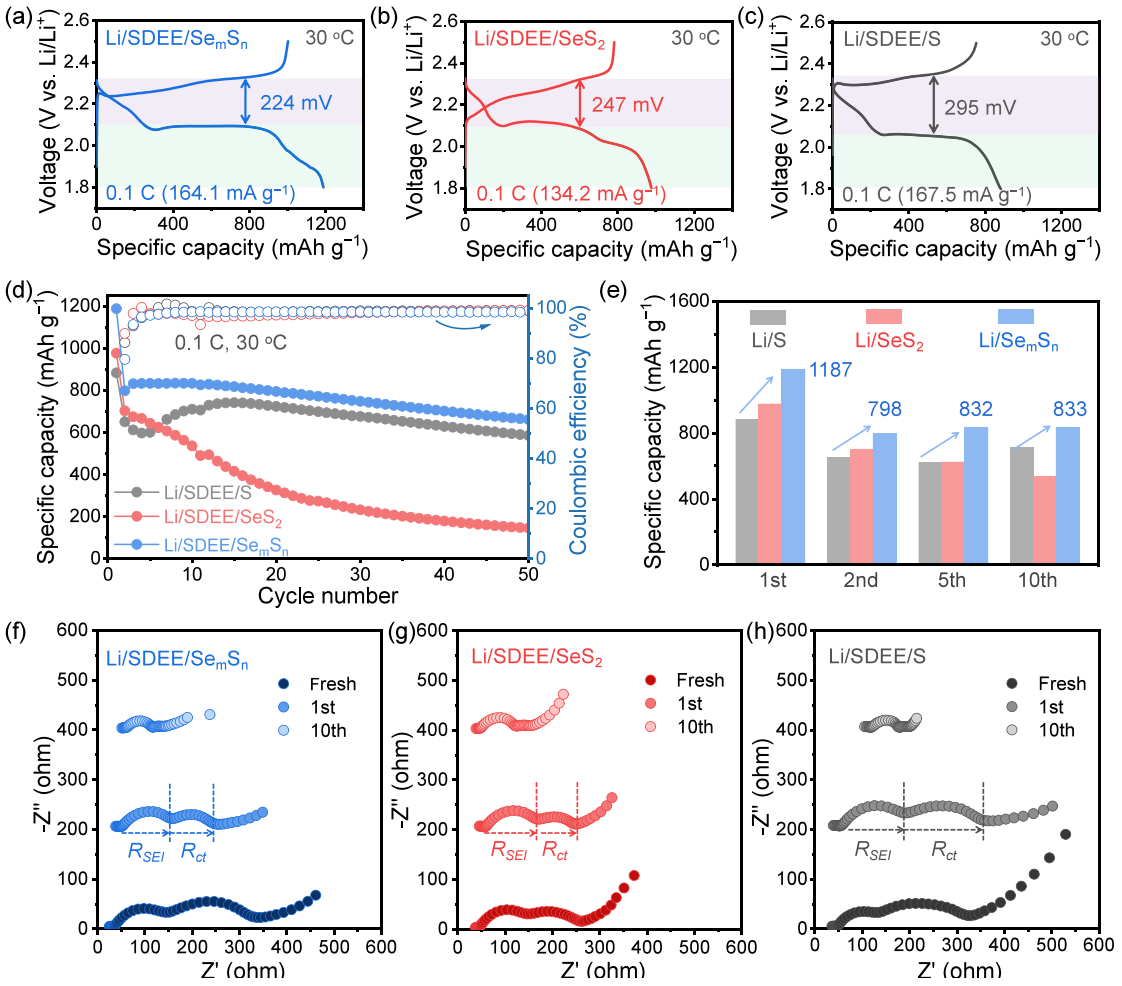


Figure 5. Electrochemical performances of LCBs using various cathodes with an SDEE at 30 °C. Galvanostatic charge−discharge profiles of (a) Li/Se_mS_n, (b) Li/SeS_2, and (c) Li/S batteries with an SDEE under 0.1 C at 30 °C. The comparison of (d) cycling performance and (e) specific capacities of LCBs with an SDEE. Nyquist plots of (f) Li/Se_mS_n, (g) Li/SeS_2, and (h) Li/S batteries after various cycles. Note: 1 C was defined as 1641, 1342, and 1675 mA g^{-1} for Li/Se_mS_n, Li/SeS_2, and Li/S cells, respectively. R_{SEI} refers to resistance of the SEI layer. R_{ct} refers to resistance of charge transfer.

electrolytes for lithium/sulfur batteries is shown in Table S3 in the Supporting Information. Moreover, two well-defined cathodic peaks at ∼2.24 V and ∼2.07 V are observed in the Li/SDEE/Se_mS_n cell (Figure S15, Supporting Information), corresponding to stepwise reduction of Se_mS_n to soluble polysulfides/polyselenides and their further conversion to Li_2S/Li_2Se, respectively. The sharp anodic peak at ∼2.35 V indicates a single-step, complete oxidation back to the original chalcogenide, which is consistent with the low overcharging degree of 8.4% and effective shuttle suppression. In stark contrast, the ether-based Li/Se_mS_n cell displays a broad anodic peak at ∼2.28 V, a hallmark of the polysulfide/polyselenide shuttle where soluble intermediates cross over to the anode and are reoxidized. The Li@IL cell shows sluggish kinetics with larger peak-to-peak separation (cathodic peak at ∼2.19 V and anodic peak at ∼2.35 V), indicative of high charge-transfer resistance because of the high viscosity of the Li@IL electrolyte. The small polarization and sharp peaks in the SDEE confirm that the moderate solvation structure facilitates faster electrode kinetics while preventing active material dissolution. At 80 °C, the SDEE-based Li/Se_mS_n cell exhibits an overcharging degree of 42.4% (Figures S16 and S17, Supporting Information), which remains lower than the ether-based cell at 60 °C. This indicates that the SDEE still provides some degree of shuttle-effect suppression even at this elevated temperature. Nevertheless, the overcharging is substantially larger than the 8.4% observed at 60 °C, and the capacity fades more rapidly, revealing that the electrolyte's effectiveness is markedly reduced under these more aggressive conditions. The SDEE-based cell also demonstrates improved rate capability and better reversibility compared to the ether-based and Li@IL-based cells (Figures S18−S20, Supporting Information). Although the SDEE can mitigate the shuttle effect at moderately elevated temperatures (e.g., 60 °C), further electrolyte optimization is required for stable long-term operation at 80 °C and above.

To evaluate the effect of electrolytes on the stabilization of lithium metal anodes, symmetric Li/Li cells with the SDEE and ether-based electrolytes were assembled and tested at elevated temperatures. The Li/Li cells were measured at a current density of 0.25 mA cm^{-2} (0.25 mAh cm^{-2}) at 60 °C (Figure S21, Supporting Information). As shown in Figure 4a, the cycled Li metal anode in the SDEE exhibits a compact and flat morphology, suggesting uniform lithium deposition during charging and discharging, which is attributed to fast lithium-ion transport in the SDEE. In contrast, a Li metal anode in a

https://doi.org/10.1021/acs.nanolett.6c03111
Nano Lett. 2026, 26, 11538−11547

Downloaded from pubs.acs.org/naleftd/article-pdf/26/34/11538/6946057/acs.nanolett.6c03111.pdf by SOUTHWEST JIAOTONG UNIV user on 07 November 2026

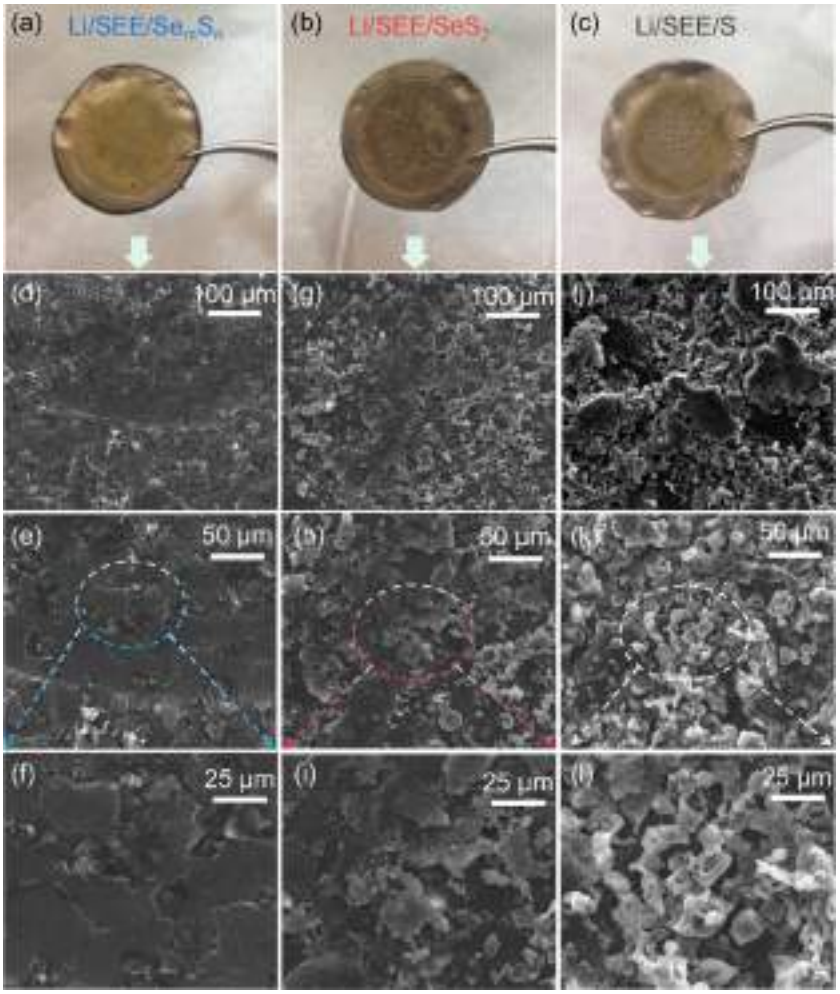


Figure 6. Microstructural analysis of cycled lithium metal anodes in SDEE-based LCBs with different cathodes at 30 °C. Digital photos of Li metal anodes in (a) Li/Se$_m$S$_n$, (b) Li/SeS$_2$, and (c) Li/S cells. Corresponding SEM images of Li metal anodes in (d–f) Li/Se$_m$S$_n$, (g–i) Li/SeS$_2$, and (j–l) Li/S cells. Note: All LCBs were disassembled after 50 cycles under 0.1 C at 30 °C.

conventional ether-based electrolyte shows a rough surface with mossy Li dendrites (Figure 4b), indicating nonuniform lithium deposition because of the sluggish Li^+ ion transport. Furthermore, the mossy Li dendrites show obvious detachment from the lithium metal substrate (Figure S22, Supporting Information). This instability, coupled with the repeated formation of a thick and inhomogeneous SEI layer, leads to continuous consumption of active lithium and the generation of dead Li. However, in a full cell with a substantial excess of lithium metal, the CE is primarily governed by cathode-side shuttle effects of polysulfides/polyselenides, which causes irreversible loss of active material and parasitic reactions at the anode. Therefore, the low CE observed in the Li/Se$_m$S$_n$ cell with an ether-based electrolyte (Figure 3h) is mainly attributed to the unmitigated shuttle effect, consistent with the pronounced overcharging and rapid capacity fade, while the nonuniform Li deposition and unstable SEI further degrade the lithium anode and aggravate the overall performance decay.

To further confirm the impact of ion solvation structure on SEI formation, depth-resolved X-ray photoelectron spectroscopy (XPS) was performed on cycled lithium metal anodes (Figures S23–S25, Supporting Information). Quantitative atomic concentration profiles as a function of etching time reveal a striking contrast between the SDEE and ether-based electrolyte. On the lithium surface cycled in the SDEE, a high and nearly depth-independent LiF content is observed (Figure 4c,e), demonstrating the formation of a uniform, anion-derived SEI that originates from the preferential decomposition of $TFSI^-$ within the CIP-dominated solvation structure.[39] In contrast, the lithium anode from the ether-based electrolyte exhibits a surface rich in organic species (C–C, C–O, R–C=O) that gradually diminish with depth (Figure 4d,f), while the LiF content remains low and decreases rapidly. The robust, LiF-rich SEI formed in SDEE effectively suppresses continuous electrolyte decomposition and lithium corrosion, thereby enabling a reversible lithium metal anode, a mitigated shuttle effect, and good cycling stability of SDEE-based Li/Se$_m$S$_n$ cells at elevated temperatures (Figure 3g).

To quantitatively evaluate the reversibility of lithium plating/stripping, Li/Cu half-cell CE measurements[40] were further performed at 60 °C at a current density of 0.33 mA cm^{-2} with a fixed areal capacity of 0.5 mAh cm^{-2} (Figure S26, Supporting Information). The ether-based electrolyte displays a rapidly declining CE, averaging below 40%, indicative of severe parasitic reactions and continuous electrolyte consumption at elevated temperature. In contrast, the Li/Cu cell employing SDEE achieves an average CE above 60%, demonstrating notably improved lithium utilization and reduced irreversible side reactions. While this value still leaves room for optimization, the clear superiority over the ether

https://doi.org/10.1021/acs.nanolett.6c03111
Nano Lett. 2026, 26, 11538–11547

Downloaded from pubs.acs.org/naleft/article-pdf/26/34/11538/6946057/acs.nanolett.6c03111.pdf by SOUTHWEST JIAOTONG UNIV user on 07 November 2026

control provides direct evidence that the sulfonamide eutectic system enables a more stable solid-electrolyte interphase and more reversible lithium plating/stripping. These results underscore the potential of SDEE for high-temperature LCBs and indicate that further refinement of the electrolyte formulation to enhance lithium metal anode stability is a worthwhile direction for future investigation.

To evaluate the suitability of SDEE for LCBs with different cathode materials, we further assembled and tested the SDEE-based LCBs with Se_mS_n, selenium disulfide (SeS_2), and sulfur (S) cathodes at ambient temperature. The initial galvanostatic charge−discharge profiles of the SDEE-based LCBs (Figure 5a−c) show no overcharging behavior even at a low rate of 0.1 C, demonstrating the effective suppression of the polysulfides/polyselenides shuttle effect during cycling. Notably, the Li/Se_mS_n cell delivers a higher specific discharge capacity (~1187 mAh g^{-1} at 0.1 C) compared to Li/SeS_2 (~976 mAh g^{-1}) and Li/S (~883 mAh g^{-1}) cells, indicating a higher utilization of active material within Se_mS_n. Furthermore, the Li/SDEE/Se_mS_n cell exhibits the smallest polarization overpotential (224 mV) than that of Li/SeS_2 (247 mV) and Li/S (295 mV) cells, which is attributed to enhanced redox reaction kinetics by combining sulfur and selenium. Consequently, the Li/SDEE/Se_mS_n cell exhibits stable cyclability with a high CE of 98.4% (Figure 5d,e), indicating a reversible lithium metal anode during cycling. To gain further insight into the interfacial kinetics and charge transfer resistance of the SDEE-based LCBs, electrochemical impedance spectroscopy (EIS) was conducted after various cycles (Figure 5f−h and Table S2, Supporting Information). When compared with the other two cells, the Li/SDEE/Se_mS_n cell exhibits a markedly smaller diameter for both SEI resistance (R_{SEI}) and charge-transfer resistance (R_{ct}), which suggests the formation of a more stable and conductive SEI layer on the lithium metal anode during the initial cycle.

We note that the active material loading employed in this study (1.0−1.5 mg cm^{-2}) is relatively modest and the electrolyte-to-sulfur ratio (34 μL mg^{-1}) is high, reflecting the high viscosity of the SDEE, which can restrict electrolyte infiltration at elevated areal capacities. Nevertheless, the pronounced suppression of the shuttle effect was evidenced by the exceptionally low overcharging degree of 8.4% and a CE of 97.2% at 60 °C. These results demonstrate promising potential of the SDEE for future high-energy LCBs and lay the foundation for practical development. Future efforts will focus on reducing electrolyte viscosity through the incorporation of fluorinated ether diluents, as already proposed, and optimizing cathode pore structures to enable higher sulfur loadings without sacrificing the unique shuttle-suppression capability.

Additionally, postcycling analysis of lithium metal anodes after 50 cycles reveals the critical impact of cathode materials on anode stability in SDEE-based LCBs (Figure 6). The anode from the Li/Se_mS_n cell shows a smooth and dense surface, indicating a stable SEI and minimal side reactions (Figure 6a,d−f). In contrast, a lithium metal anode paired with a SeS_2 cathode exhibits bulk-like, mossy Li deposits, leading to active Li loss and rapid capacity fade (Figure 6b,g−i). However, despite better cycling stability than the Li/SeS_2 cell, the SDEE-based Li/S cell shows the most severe failure of the lithium anode (i.e., a thick, porous Li deposition layer) coupled with obvious yellow discoloration on the separator and cathode (Figure 6c,j−l and Figure S27, Supporting Information). This observation further confirms a severe polysulfides/polyselenides shuttling effect and degradation of the lithium anode during cycling, which is well consistent with the much increased ohmic resistance in Figure 5h. These results demonstrate that the rational design of sulfur−selenium cathodes to harness their combined advantages is therefore essential for achieving stable, high-performance lithium metal batteries with an SDEE.

In summary, this study establishes a rational electrolyte design framework for high-temperature lithium−chalcogenide batteries based on a nonflammable sulfonamide deep eutectic electrolyte (SDEE). Through systematic compositional tuning, we demonstrate that a homogeneous electrolyte with a CIP-dominated solvation structure is formed at the optimal DMMSA:LiTFSI ratio of 4:1. This moderate solvation environment of the SDEE provides sufficient Li^+ coordination to achieve complete salt dissociation and a high lithium-ion transference number, while the relatively weak solvent−Li^+ interaction minimizes dissolution of the active material and polysulfide/polyselenide intermediates, thereby suppressing the shuttle effect. Temperature-dependent Raman spectroscopy further reveals that this CIP-dominated solvation shell remains structurally intact up to 80 °C, in stark contrast to conventional ether electrolytes, which suffer from solvent evaporation and ion aggregation. The resulting electrolyte enables compact and uniform lithium deposition, as well as an improved Coulombic efficiency in Li/Cu half-cells compared to the ether baseline. When benchmarked against a representative nonflammable ionic liquid, the SDEE delivers superior capacity utilization while retaining inherent safety and a significant cost advantage, highlighting the unique value proposition of the SDEE. We envision that the design concept of leveraging thermally stable, moderately solvating eutectic systems can be generalized to other dissolution-plagued electrode chemistries and will stimulate further exploration of functional hydrogen-bond donors for next-generation safe, high-energy batteries operating under extreme conditions.

■ ASSOCIATED CONTENT

Supporting Information

The Supporting Information is available free of charge at https://pubs.acs.org/doi/10.1021/acs.nanolett.6c03111.

DSC and LSV curves of the sample; digital photos of electrolyte samples; Raman spectra of samples at different temperatures; DFT calculation results of electrolytes; lithium-ion transference number measurement of electrolyte samples; flammability tests of a Li@IL electrolyte; TGA curve and ICP-OES results of Se_mS_n@C composites; electrochemical performances of LCBs; SEM images and XPS analysis of cycled lithium metal anodes with different electrolytes; voltage profiles of Li/Cu cells; SEM images of cycled cathodes; impedance of LCBs with different electrolytes; comparison of electrochemical performance of reported Li/S batteries at elevated temperature (PDF)

■ AUTHOR INFORMATION

Corresponding Authors

Min-Kyu Song − *School of Mechanical and Materials Engineering, Washington State University, Pullman, Washington 99164, United States;* orcid.org/0000-0002-8998-3853; Email: minkyu.song@wsu.edu

Weiqing Yang − *Research Institute of Frontier Science and Key Laboratory of Advanced Technologies of Materials (Ministry*

https://doi.org/10.1021/acs.nanolett.6c03111
Nano Lett. 2026, 26, 11538−11547

Downloaded from pubs.acs.org/naleld/article-pdf/26/34/11538/6946057/acs.nanolett.6c03111.pdf by SOUTHWEST JIAOTONG UNIV user on 07 November 2026

of Education), School of Materials Science and Engineering, Southwest Jiaotong University, Chengdu 610031, China; orcid.org/0000-0001-8828-9862; Email: wqyang@swjtu.edu.cn

Authors

Panpan Dong − *Research Institute of Frontier Science and Key Laboratory of Advanced Technologies of Materials (Ministry of Education), School of Materials Science and Engineering, Southwest Jiaotong University, Chengdu 610031, China;* orcid.org/0000-0002-2349-5988

Xuemeng Gan − *Key Laboratory of Advanced Technologies of Materials (Ministry of Education), School of Materials Science and Engineering, Southwest Jiaotong University, Chengdu 610031, China*

Liangjie Gu − *Key Laboratory of Advanced Technologies of Materials (Ministry of Education), School of Materials Science and Engineering, Southwest Jiaotong University, Chengdu 610031, China*

Ting Yang − *Key Laboratory of Advanced Technologies of Materials (Ministry of Education), School of Materials Science and Engineering, Southwest Jiaotong University, Chengdu 610031, China*

Muqiao Su − *School of Mechanical and Materials Engineering, Washington State University, Pullman, Washington 99164, United States*

Complete contact information is available at: https://pubs.acs.org/10.1021/acs.nanolett.6c03111

Notes

The authors declare no competing financial interest.

■ ACKNOWLEDGMENTS

This work was supported by the Fundamental Research Funds for the Central Universities (No. 2682026GH006), Sichuan Science and Technology Program (No. 2025ZNSFSC1413), Start-up Research Funding of Southwest Jiaotong University (No. 2682024KJ003), and Postdoctoral Fellowship Program of China Postdoctoral Science Foundation (No. GZC20241407). The authors thank the Analysis & Testing Center at Southwest Jiaotong University for use of SEM and XPS measurements.

■ REFERENCES

(1) Lin, X.; Salari, M.; Arava, L. M. R.; Ajayan, P. M.; Grinstaff, M. W. High temperature electrical energy storage: advances, challenges, and frontiers. *Chem. Soc. Rev.* **2016**, *45* (21), 5848−5887.

(2) Feng, Y.; Zhou, L.; Ma, H.; Wu, Z.; Zhao, Q.; Li, H.; Zhang, K.; Chen, J. Challenges and advances in wide-temperature rechargeable lithium batteries. *Energy Environ. Sci.* **2022**, *15* (5), 1711−1759.

(3) Duan, J.; Tang, X.; Dai, H.; Yang, Y.; Wu, W.; Wei, X.; Huang, Y. Building Safe Lithium-Ion Batteries for Electric Vehicles: A Review. *Electrochemical Energy Reviews* **2020**, *3* (1), 1−42.

(4) Eftekhari, A. The rise of lithium-selenium batteries. *Sustainable Energy & Fuels* **2017**, *1* (1), 14−29.

(5) Chen, Z.; Zhi, C. Chalcogens for high-energy batteries. *Nature Reviews Materials* **2025**, *10* (4), 268−284.

(6) Hua, W.; Li, H.; Pei, C.; Xia, J.; Sun, Y.; Zhang, C.; Lv, W.; Tao, Y.; Jiao, Y.; Zhang, B.; Qiao, S.-Z.; Wan, Y.; Yang, Q.-H. Selective Catalysis Remedies Polysulfide Shuttling in Lithium-Sulfur Batteries. *Adv. Mater.* **2021**, *33* (38), 2101006.

(7) Tian, H.; Tian, H.; Wang, S.; Chen, S.; Zhang, F.; Song, L.; Liu, H.; Liu, J.; Wang, G. High-power lithium-selenium batteries enabled by atomic cobalt electrocatalyst in hollow carbon cathode. *Nat. Commun.* **2020**, *11* (1), 5025.

(8) Huang, L.; Li, J.; Liu, B.; Li, Y.; Shen, S.; Deng, S.; Lu, C.; Zhang, W.; Xia, Y.; Pan, G.; Wang, X.; Xiong, Q.; Xia, X.; Tu, J. Electrode Design for Lithium-Sulfur Batteries: Problems and Solutions. *Adv. Funct. Mater.* **2020**, *30* (22), 1910375.

(9) Feng, J.; Yu, S.; Shi, C.; Tang, X.; Zhao, X.; Chen, S.; Song, J. Advanced Cathode Designs for High-Energy Lithium/Sodium-Selenium Battery. *Adv. Funct. Mater.* **2025**, *35* (24), 2422013.

(10) Guo, Y.; Zhu, S.; Mao, C.; Chen, Y.; Liu, L.; Liu, J.; Wang, X.; Wu, Q.; Yang, L.; Hu, Z. High-Rate Lithium-Selenium Batteries Boosted by a Multifunctional Janus Separator Over a Wide Temperature Range of −30 to 60 °C. *Adv. Mater.* **2023**, *35* (46), 2304551.

(11) Xia, S.; Xu, X.; Wu, W.; Chen, Y.; Liu, L.; Wang, G.; Fu, L.; Zhang, Q.; Wang, T.; He, J.; Wu, Y. Advancements in functionalized high-performance separators for lithium-sulfur batteries. *Materials Science and Engineering: R: Reports* **2025**, *163*, 100924.

(12) Zhou, Y.; Li, Z.; Lu, Y.-C. A stable lithium-selenium interface via solid/liquid hybrid electrolytes: Blocking polyselenides and suppressing lithium dendrite. *Nano Energy* **2017**, *39*, 554−561.

(13) Dong, P.; Zhang, X.; Cha, Y.; Lee, J.-I.; Song, M.-K. In situ surface protection of lithium metal anode in Lithium-Selenium disulfide batteries with ionic liquid-based electrolytes. *Nano Energy* **2020**, *69*, 104434.

(14) Zhao, H.; Deng, N.; Yan, J.; Kang, W.; Ju, J.; Ruan, Y.; Wang, X.; Zhuang, X.; Li, Q.; Cheng, B. A review on anode for lithium-sulfur batteries: Progress and prospects. *Chemical Engineering Journal* **2018**, *347*, 343−365.

(15) Nanda, S.; Asl, H. Y.; Bhargav, A.; Manthiram, A. Thiometallate-mediated polysulfide chemistry and lithium stabilization for stable anode-free lithium-sulfur batteries. *Cell Reports Physical Science* **2022**, *3* (4), 100808.

(16) Jung, S.-Y.; Chen, Y.-P.; Lee, Y.-J.; Kim, S. H.; Bae, J.-S.; Chen, X.; Yu, S.-H. Low-polarity solvent-mediated lithium metal stabilization for improved performance in lithium-sulfur batteries. *Journal of Energy Chemistry* **2026**, *114*, 737−749.

(17) Kim, J. H.; Kim, M.; Kim, S.-J.; Kim, S.-Y.; Yu, S.; Hwang, W.; Kwon, E.; Lim, J.-H.; Kim, S. H.; Sung, Y.-E.; Yu, S.-H. Understanding the electrochemical processes of SeS_2 positive electrodes for developing high-performance non-aqueous lithium sulfur batteries. *Nat. Commun.* **2024**, *15* (1), 7669.

(18) Hua, X.; Zhang, T.; Offer, G. J.; Marinescu, M. Towards online tracking of the shuttle effect in lithium sulfur batteries using differential thermal voltammetry. *Journal of Energy Storage* **2019**, *21*, 765−772.

(19) Deng, D.-R.; Xiong, H.-J.; Luo, Y.-L.; Yu, K.-M.; Weng, J.-C.; Li, G.-F.; Lei, J.; Li, Y.; Zheng, M.-S.; Wu, Q.-H. Accelerating the Rate-Determining Steps of Sulfur Conversion Reaction for Lithium-Sulfur Batteries Working at an Ultrawide Temperature Range. *Adv. Mater.* **2024**, *36* (39), 2406135.

(20) Li, B.; Jiang, W.; Qu, Y.; Song, W.; Jin, X.; Pei, M.; Zhuo, S.; Mao, R.; Wang, L.; Liu, D.; Jian, X.; Hu, F. Molecular Engineering of Polymer Brushes Enables Lithium-Sulfur Battery Stable Operation under Ultra-Wide Temperature Range. *Adv. Mater.* **2025**, *37* (35), 2503482.

(21) Qu, W.; Xia, J.; Luo, C.; Zhang, C.; Chen, R.; Lv, W.; Yang, Q. Lithium-Sulfur Batteries at Extreme Temperatures: Challenges, Strategies and Prospects. *Energy & Environmental Materials* **2023**, *6* (4), No. e12444.

(22) Zhang, H.; Chen, J.; Li, Z.; Peng, Y.; Xu, J.; Wang, Y. Operating Lithium-Sulfur Batteries in an Ultrawide Temperature Range from −50 to 70 °C. *Adv. Funct. Mater.* **2023**, *33* (48), 2304433.

(23) Xu, G.-L.; Sun, H.; Luo, C.; Estevez, L.; Zhuang, M.; Gao, H.; Amine, R.; Wang, H.; Zhang, X.; Sun, C.-J.; Liu, Y.; Ren, Y.; Heald, S. M.; Wang, C.; Chen, Z.; Amine, K. Solid-State Lithium/Selenium-Sulfur Chemistry Enabled via a Robust Solid-Electrolyte Interphase. *Adv. Energy Mater.* **2019**, *9* (2), 1802235.

(24) Wang, D.; Jhang, L.-J.; Kou, R.; Liao, M.; Zheng, S.; Jiang, H.; Shi, P.; Li, G.-X.; Meng, K.; Wang, D. Realizing high-capacity all-solid-

Downloaded from pubs.acs.org/naletd/article-pdf/26/34/11538/6946057/acs.nanolett.6c03111.pdf by SOUTHWEST JIAOTONG UNIV user on 07 November 2026

state lithium-sulfur batteries using a low-density inorganic solid-state electrolyte. *Nat. Commun.* **2023**, *14* (1), 1895.
(25) Mendes, T. C.; Nguyen, C.; Barlow, A. J.; Cherepanov, P. V.; Forsyth, M.; Howlett, P. C.; MacFarlane, D. R. A safe Li-Se battery in an ionic liquid-based electrolyte operating at 25−70 °C by using a N,S,O tri-doped mesoporous carbon host material. *Sustainable Energy & Fuels* **2020**, *4* (5), 2322−2332.
(26) Hu, S.; Zhang, H.; Li, Y.; Sun, R.; Zhang, X.; Yi, M.; Zuo, Y.; Pang, H. Ionic-Liquid-Triggered Amorphization Engineers Symmetry-Breaking p-Block Bismuth Oxides with Electric Dipole Domains for Practical Lithium-Sulfur Batteries. *Adv. Mater.* **2026**, *38* (36), No. e73469.
(27) Gao, Y.; Zhu, L.; Wang, B.; Xu, Y.; Chai, J.; Fu, A.; Li, H.; Li, J.; Peng, Y.; Zheng, Y.; Wang, Y.; Lee, J. Y.; Lv, D.; Liu, Z. Molecular Engineering Enabled Stable Deep Eutectic Amide-Based Electrolyte for High-Temperature Lithium-Metal Batteries. *ACS Energy Letters* **2024**, *9* (8), 3931−3938.
(28) Pu, Y.; Wang, Q.; Dou, R.; Ren, X.; Lu, L. A crown-ether-enabled eutectic electrolyte for ultra-high temperature lithium metal batteries. *Energy Storage Materials* **2024**, *67*, 103285.
(29) Kumaravel, V.; Bartlett, J.; Pillai, S. C. Solid Electrolytes for High-Temperature Stable Batteries and Supercapacitors. *Adv. Energy Mater.* **2021**, *11* (3), 2002869.
(30) Park, J.-W.; Ueno, K.; Tachikawa, N.; Dokko, K.; Watanabe, M. Ionic Liquid Electrolytes for Lithium-Sulfur Batteries. *J. Phys. Chem. C* **2013**, *117* (40), 20531−20541.
(31) Guzmán-González, G.; Alvarez-Tirado, M.; Olmedo-Martínez, J. L.; Picchio, M. L.; Casado, N.; Forsyth, M.; Mecerreyes, D. Lithium Borate Ionic Liquids as Single-Component Electrolytes for Batteries. *Adv. Energy Mater.* **2023**, *13* (1), 2202974.
(32) Fang, M.; Yue, X.; Dong, Y.; Chen, Y.; Liang, Z. A temperature-dependent solvating electrolyte for wide-temperature and fast-charging lithium metal batteries. *Joule* **2024**, *8* (1), 91−103.
(33) Li, Y.; Huang, Y.; Han, X.; Wu, J.; Shen, H.; Wang, S.; Ding, S.; Zhu, S.; Han, B.; Huang, Y.; Zhang, D.; Xue, W. Temperature-Adaptive Fluorine in Electrolyte for Lithium-Metal Batteries at Low Temperatures. *ACS Energy Letters* **2025**, *10* (7), 3610−3619.
(34) Phan, A. L.; Nan, B.; Le, P. M. L.; Miao, Q.; Wu, Z.; Le, K.; Chen, F.; Engelhard, M.; Dan Nguyen, T.; Han, K. S.; Heo, J.; Zhang, W.; Baek, M.; Xu, J.; Zhang, X.; Liu, P.; Ma, L.; Wang, C. Lightweight Electrolyte Design for Li/Sulfurized Polyacrylonitrile (SPAN) Batteries. *Adv. Mater.* **2024**, *36* (35), 2406594.
(35) Phan, A. L.; Le, P. M. L.; Wang, C. Realizing high-energy and long-life Li/SPAN batteries. *Joule* **2024**, *8* (6), 1601−1618.
(36) Huang, X.; Huang, S.; Wang, T.; Zhong, L.; Han, D.; Xiao, M.; Wang, S.; Meng, Y. Polyether-b-Amide Based Solid Electrolytes with Well-Adhered Interface and Fast Kinetics for Ultralow Temperature Solid-State Lithium Metal Batteries. *Adv. Funct. Mater.* **2023**, *33* (27), 2300683.
(37) Song, X.; Zhang, Y.; Guo, Z.; Wu, S.; Zhao, Y.; Liang, X.; Kim, M.-C.; Kim, H.; Sun, Y.-K. Lithium-Bond-Based Deep Eutectic Electrolyte Solutions for High-Temperature Lithium Metal Batteries. *Angew. Chem., Int. Ed.* **2025**, *64* (39), No. e202511772.
(38) Zhao, C.; Daali, A.; Hwang, I.; Li, T.; Huang, X.; Robertson, D.; Yang, Z.; Trask, S.; Xu, W.; Sun, C.-J.; Xu, G.-L.; Amine, K. Pushing Lithium-Sulfur Batteries towards Practical Working Conditions through a Cathode-Electrolyte Synergy. *Angew. Chem., Int. Ed.* **2022**, *61* (27), No. e202203466.
(39) He, Y.; Wang, L.; Wang, A.; Zhang, B.; Pham, H.; Park, J.; He, X. Insight into uniform filming of LiF-rich interphase via synergistic adsorption for high-performance lithium metal anode. *Exploration* **2024**, *4* (2), 20230114.
(40) Adams, B. D.; Zheng, J.; Ren, X.; Xu, W.; Zhang, J.-G. Accurate Determination of Coulombic Efficiency for Lithium Metal Anodes and Lithium Metal Batteries. *Adv. Energy Mater.* **2018**, *8* (7), 1702097.

Downloaded from pubs.acs.org/naleftd/article-pdf/26/34/11538/6946057/acs.nanolett.6c03111.pdf by SOUTHWEST JIAOTONG UNIV user on 07 November 2026

https://doi.org/10.1021/acs.nanolett.6c03111
Nano Lett. 2026, 26, 11538−11547